Photoionization of atomic barium subshells in the 4d threshold region using the relativistic multiconfiguration Tamm-Dancoff approximation

Aarthi Ganesan, P. C. Deshmukh, and S. T. Manson

Phys. Rev. A **95**, 033417 — Published 17 March 2017

DOI: 10.1103/PhysRevA.95.033417

Photoionization of Atomic Barium Subshells in the 4d threshold Region using the Relativistic Multi-Configuration Tamm-Dancoff Approximation

Aarthi Ganesan[1], P. C. Deshmukh[2, 3] and S. T. Manson[4]

1] Department of Physics, Centre for Post-Graduate Studies, Jain University, Bengaluru 560011, India
2] Department of Physics, Indian Institute of Technology Tirupati, Tirupati, 517506, India
3] Department of Physics, Indian Institute of Science Education and Research, Tirupati, 517507, India
4] Department of Physics and Astronomy, Georgia State University, Atlanta, GA 30303, USA

Abstract: Photoionization cross sections and photoelectron angular distribution asymmetry parameters are calculated for the $4d^{10}$, $5s^2$, $5p^6$ and $6s^2$ subshells of atomic barium as a test of the relativistic multiconfiguration Tamm-Dancoff (RMCTD) method. The shape resonance present in the near-threshold region of the 4d subshell is studied in detail in the 4d photoionization along with the 5s, 5p and 6s subshells in the region of the 4d thresholds, as the 4d shape resonance strongly influences these subshells in its vicinity. The results are compared with available experiment and other many-body theoretical results in an effort to assess the capabilities of the RMCTD methodology. The electron correlations addressed in the RMCTD method give relatively good agreement with the experimental data, indicating that the important many-body correlations are included correctly.

I. Introduction

The study of the photoionization atomic barium subshells has interested many over the last few decades [1-9]. Barium is an interesting many-body system to examine the combined effects of relativistic and correlation interactions since (a) it is a high-Z system so that relativistic (primarily spin-orbit) interactions play an important role, (b) the outer $6s^2$ subshell is known to be highly correlated, (c) the large photoionization cross section of the inner 4d subshell of barium, which undergoes a delayed maxima (shape resonance), strongly affects other nearby subshell cross sections *via* correlation in the form of interchannel coupling, and (d) sufficient experimental data [5-8] are available for atomic barium, with which theoretical results can be compared and assessed.

As is well-known, the physics of the atomic photoionization process generally goes well beyond the description by the independent particle approximation since the many-electron correlations are important [10, 11]. Even a non-relativistic many-body theory is often inadequate. Among successful relativistic many-body methods, the Relativistic Random Phase Approximation (RRPA) [12] and the Relativistic Multi-Configuration Tamm-Dancoff (RMCTD) methods [13] include both relativistic and many-body correlation effects. The RRPA has been found to be

quite successful in a number of different situations, for example in the photoionization study of noble gas atoms [12 - 16], several other closed shell atoms from Group IIA [17-19], IIB [20-22], and also Pd, Yb, Rd [23, 24, 25]. It has also been used with considerable success to account for photoionization of closed-shell negative ions. In addition, the RRPA has also been used along with the Relativistic Multichannel Quantum Defect theory [26] to understand autoionization resonances [27, 28] in atomic systems. Notwithstanding the success of the RRPA method, it must be mentioned that even as it includes some of the most important electron correlations, the RRPA leaves out the correlations that come from the ionization plus excitation channels. The RMCTD method takes into account electron correlations in both the initial state and the final state of photoionization, like the RRPA, but differs from it in some details. Even as both RRPA and the RMCTD take into account electron correlations in the final state *via* interchannel coupling, the initial state correlations are included in the RRPA method by summing over all ring (and corresponding exchange) diagrams, whereas in the RMCTD method, the initial state correlations are included *via* explicit configuration interaction, by obtaining the initial state wavefunctions using GRASP-92 [29] to generate Multi-Configuration Dirac-Hartree-Fock (MCDF) wavefunctions. This difference enables the application of the RMCTD method to take account of ionization-plus-excitation channels *not* included in the RRPA, and from all the configurations which are explicitly included in the MCDF wavefunction. Unfortunately, there are only a few studies in which the RMCTD method has been tested. For example, it has been used to account for photoionization of a very few atoms, Mg and Be [13], Cd [30] and Xe [31] and photodetachment of a few negative ions [32, 33]. The present study tests the applicability of the RMCTD to a rather highly correlated atom, atomic barium. Salient features of the RMCTD method are reviewed in Section II below.

Various theoretical and experimental photoionization studies of atomic barium have been reported. On the experimental side, Bizau *et al*., [6] have reported X-ray photoelectron spectrometry (XPS) study of photoionization in atomic barium subshells using synchrotron radiation between 16 and 180 eV photon energy. Snell *et al.,* [34] have measured the 4d and 5p photoelectron spectra of atomic barium using *narrow-band-width* synchrotron radiation of 131.2eV photon energy. Whitfield *et al.,* [8] have reported the angular distribution and the photoionization cross section of Ba 5s in the energy region of the second Cooper minimum, from 120 to 260eV. The outer $6s^2$ subshell of Ba is very strongly mixed with $6p^2$ and $5d^2$, and hence single-particle calculations, e.g., Hartree-Fock and Dirac-Hartree-Fock, of the ground state are inadequate. Theoretical studies of atomic barium have been done using Hartree-Fock (HF)

wavefunctions, both with and without relaxation, by Kelly *et al.,* [4], the Random Phase Approximation with Exchange (RPAE) [1], the Relativistic Random Phase Approximation (RRPA) [12], RRPA *with* relaxation (RRPA-R) [2] and Many-Body Perturbation Theory (MBPT) [3]. Kutzner *et al.* [3] have reported photoionization cross sections and angular distribution asymmetry parameters for inner and outer subshells of barium including relaxation and polarization effects using MBPT. They used two different methods to include relaxation and polarization effects: one by taking into account the higher-order diagrams in MBPT and the other by calculating the excited state wave functions in the potential of a relaxed ionic core. The MBPT results were found to be in good agreement with the available experimental data.

Thus, in contradistinction to the case of Xe [14], where methodologies like RRPA [12] work quite well, Ba requires far more in the way of correlation included to achieve quantitative accuracy, certainly more than is included in RRPA or RPAE, its nonrelativistic counterpart. This then offers an excellent case for the testing of the capabilities of the relativistic multiconfiguration Tamm-Dancoff approximation (RMCTD) method. In the present work, we focus on the photoionization in the energy region of the shape resonance in the 4d subshell cross section of atomic barium where both initial and final state correlations are important. Non-RPA correlations are included in the present work by mixing other important configurations in the initial state using the RMCTD method. The dipole channels from the excited state configurations to the continuum, along with the channels to the bound excited states, make this approach powerful to address electron correlations involved in the photoionization process. We report results using the RMCTD methodology and compare with results obtained using RRPA and RRPA-R methods, and also with available experimental data. Photoionization from 4d, 5s, 5p and 6s subshells of barium are studied in the energy region in the neighborhood of the 4d thresholds.

II. Theory

The multiconfiguration initial state wavefunction for RMCTD method is obtained using the *General Purpose Relativistic Atomic Structure Program* (GRASP92) [29]. GRASP92 is a suite of programs for calculating atomic energy levels, oscillator strengths and discrete wavefunctions using a fully relativistic approach. The radial charge density of the nucleus is calculated based on the Fermi statistical distribution function. The α^{th} Atomic State Function (ASF) for an N-electron system is a linear combination of the n_c number of electronic Configuration State Functions

(CSF) [35], expressed as $\Psi_{\alpha}^{PJM} = \sum_{i=1}^{n_c} C_{i\alpha} \Phi_i^{PJM}$,where P (parity), J and M (total and azimuthal angular momenta) are symmetry labels. The CSFs (Φ_i^{PJM}) are linear combinations of N-electron Slater determinants made up of the four component bi-spinors, N being the number of initial state electrons. The *five* explicit configurations included in the present work to describe the initial state are shown in Table I.

Table I. Initial state configurations included in the present work.

Initial state configurations included	Weight factor
(1) $[Xe]\ 6s_{1/2}{}^2$	a_1=0.964
(2) $[Xe]\ 6s_{1/2}{}^0 5d_{3/2}{}^2$	a_2=0.067
(3) $[Xe]\ 6s_{1/2}{}^0 5d_{5/2}{}^2$	a_3=0.080
(4) $[Xe]\ 6s_{1/2}{}^0 6p_{1/2}{}^2$	a_4=0.117
(5) $[Xe]\ 6s_{1/2}{}^0 6p_{3/2}{}^2$	a_5=0.211

The first configuration is the usual HF/DHF ground state and the other configurations are built on it by considering two electron excitations from 6s to 5*d* or the 6*p* subshells. The configuration mixing weight factor obtained from the MCDHF formalism for each configuration is indicated above in Table I.

The application of an external time dependent harmonic perturbation $v_+ e^{-i\omega t}$ perturbs the MCDF wavefunction. The external perturbation used in the RRPA included positive and negative frequency terms, while in RMCTD only the positive frequency term is used. The continuum orbital function $\overline{y}_a$ for a channel $a \to \overline{a}$ is the solution of the following radial integro-differential equation [13]:

$$\left(h_{\overline{a}} + V_{\overline{a}} + \varepsilon_a - \omega\right) y_{\overline{a}} = R_{\overline{a}} \quad \text{------- (1)}$$

where $h_{\overline{a}}$ is the radial free particle Dirac Hamiltonian, $V_{\overline{a}}$ is the Hartree-Fock $V(N-1)$ potential, ε_a is the eigen value of the ground state orbital (hole) a , ω is the photon energy. The inhomogeneous term $R_{\overline{a}}$ describes the interchannel coupling and can be written as

$$R_{\bar{a}} = C_{\bar{a}} + B_{\bar{a}} + L_{\bar{a}} \quad \text{------ (2)}$$

where $C_{\bar{a}}$ describes the coupling between channels, $B_{\bar{a}}$ describes the coupling with transitions $b \to b'$ between valence orbitals leading to excited-bound (XB) states and $L_{\bar{a}}$ is the term with Lagrange multipliers ensuring the orthogonality to the ground state orbitals.

The multichannel RMCTD excited-state wavefunction with total angular momentum *J, M* has the form [13, 42] expressed as

$$\psi(JM) = \sum_{i=1}^{n_c} c_i \chi(\gamma_i JM) + \sum_{\ell=1}^{n_b} b_\ell \Phi(\gamma_\ell JM) \quad \text{------ (4)},$$

where $\chi(\gamma_i JM)$ and $\Phi(\gamma_\ell JM)$ are configuration wave functions obtained from one of the initial-state configurations ("parent" configuration) by photoexciting a valence orbital (hole a) to a continuum orbital, $\bar{a}$, or to another initial vacant state (valence) orbital, respectively. γ_i and γ_j represent all *other* quantum numbers required to define the corresponding configurations uniquely. The parameters c_i and b_ℓ are the weight coefficients of the parent configuration and excited bound configuration *(XB)* composed of ground state orbitals. n_c and n_b are the number of the continuum and excited-bound configurations respectively. The weight coefficient b_ℓ corresponding to *XB* configuration is obtained by solving the system of equations

$$\sum_{\ell=1}^{n_b} \left[H_{k\ell} - (E_0 + \omega)\delta_{k\ell} \right] b_\ell = F_k, \text{ k=1,2,....,n}_b \quad \text{------- (5)}$$

where $H_{k\ell}$ is the atomic Hamiltonian matrix element $\langle \Phi(\gamma_k JM) | H | \Phi(\gamma_\ell JM) \rangle$ between two XB configurations k and ℓ and F_k corresponds to matrix element between XB configuration k and configuration corresponding to continuum channel i which is expressed as

$$F_k = -\sum_{i=1}^{n_c} H_{ki} c_i \quad \text{------ (6)}$$

where $H_{ki} = \langle \chi(\gamma_k JM) | H | \chi(\gamma_i JM) \rangle$. In Eq. (5), E_0 is the ground state energy and ω is the photon energy.

Table II gives the ionization threshold energies calculated from DHF, ΔE_{SCF} and MCDHF (GRASP92) which are used for RRPA, RRPA-R and RMCTD respectively.

Table II. Dirac-Hartree Fock, ΔE_{SCF} and MCDHF thresholds in eV along with available experiment.

Subshell	DHF	ΔE_{SCF}	MCDHF	Experiment [6, 36]
$4s_{1/2}$	279.11	272.348	278.90	
$4p_{1/2}$	220.37	213.773	220.16	
$4p_{3/2}$	204.43	198.102	204.23	
$4d_{3/2}$	106.49	100.59	106.29	101.02
$4d_{5/2}$	103.75	97.94	103.54	98.41
$5s_{1/2}$	43.63	41.824	43.45	38.06
$5p_{1/2}$	26.03	24.312	25.85	24.75
$5p_{3/2}$	23.75	22.138	23.58	22.72
$6s_{1/2}$	4.44	4.28	4.99	5.21

Tables III and IV list the ionization and excitation channels used in the present calculations. Including dipole channels from the inner subshells from all the configurations involved in the CI improves the agreement between the theory and the experiment. There are 78 bound-to-continuum relativistic dipole ionization channels arising from the 4d+5s+5p+6s+5d+6p subshells, and, in addition, there are *9* bound-to-bound excitation channels. Thus, in the present work, interchannel coupling between a total of *87* channels are included.

Table III. Bound to continuum channels

$n \rightarrow \varepsilon$ channels	Initial state configuration number	Number of channels (Total: 78)
$4d_{3/2} \rightarrow p_{1/2}, p_{3/2}, f_{5/2}$	1, 2, 3, 4, 5	15
$4d_{5/2} \rightarrow p_{3/2}, f_{5/2}, f_{7/2}$	1, 2, 3, 4, 5	15
$5s \rightarrow p_{1/2}, p_{3/2}$	1, 2, 3, 4, 5	10
$5p_{1/2} \rightarrow s_{1/2}, d_{3/2}$	1, 2, 3, 4, 5	10
$5p_{3/2} \rightarrow s_{1/2}, d_{3/2}, d_{5/2}$	1, 2, 3, 4, 5	15

$6s \rightarrow p_{1/2}, p_{3/2}$	1	2
$5d_{3/2} \rightarrow p_{1/2}, p_{3/2}, f_{5/2}$	2	3
$5d_{5/2} \rightarrow p_{3/2}, f_{5/2}, f_{7/2}$	3	3
$6p_{1/2} \rightarrow s_{1/2}, d_{3/2}$	4	2
$6p_{3/2} \rightarrow s_{1/2}, d_{3/2}, d_{5/2}$	5	3

Table IV: Bound to bound channels

Initial state configuration number	$n \rightarrow n$ 'channels	Number of channels (Total: 09)
1	$5p_{1/2} \rightarrow 5d_{3/2}$ $5p_{3/2} \rightarrow 5d_{3/2}, 5d_{5/2}$ $6s \rightarrow 6p_{1/2}, 6p_{3/2}$	5
4	$5p_{1/2} \rightarrow 6s_{1/2}$ $5p_{3/2} \rightarrow 6s_{1/2}$	2
5	$5p_{1/2} \rightarrow 6s_{1/2}$ $5p_{3/2} \rightarrow 6s_{1/2}$	2

With reference to Table III and IV, the advantages of the RMCTD method over other many-body methods are explained in detail below. In Table III, the six allowed dipole channels from the spin-orbit split 4d subshells are listed. In the RRPA, we could consider only these six channels from the 4d subshells. The RMCTD method enables the inclusion of all relativistic dipole channels from all the five explicit configurations listed in Table I. This adds up to 15 channels for the 4d subshell as opposed to the 6 channels from 4d included in the RRPA. Also, the excitation channels from 5p and 6s are included in the RMCTD method. As discussed, the RMCTD method is formulated to include ionization channels from the excited state configuration, in addition to the channels from the parent configuration. In order to understand the effects due to configuration interaction, we have done two sets of RMCTD calculations in the present work: (a) all dipole channels only from the first configuration listed in Table I, and (b) all dipole channels from all the 5 MCDHF configurations specified in Table I. The set (a) leads to interchannel coupling between 31 photoionization dipole channels (26 channels from bound-to-

continuum states and 5 channels from bound-to-excited-bound states). When all the dipole channels from the five configurations listed in Table I are considered (set b), we get interchannel coupling between 87 dipole channels, listed in Tables III and IV. Inclusion of these additional channels improves agreement with the experiment as shown in Section III.

In the present work, we report the RMCTD results of the photoionization cross-section and the photoelectron angular distribution asymmetry parameters for photoionization from various subshells of atomic barium. The relativistic electric dipole photoionization cross section is given, for the i^{th} (or l^{th}) configuration, by [12, 37]

$$\sigma_{n\kappa}^{(i,\ell)}(\omega) = \frac{4\pi^2\alpha}{3}\omega\left(\left|D_{j\to j\text{-}1}\right|^2 + \left|D_{j\to j}\right|^2 + \left|D_{j\to j+1}\right|^2\right) \qquad \text{------ (7)}$$

with the net cross section being the weighted sum of the contributions from each configuration:

$$\sigma_{n\kappa} = \sum_{i=1}^{n_c} c_i^{\,2}\sigma_{n\kappa}^{(i)} + \sum_{\ell=1}^{n_b} b_\ell^{\,2}\sigma_{n\kappa}^{(\ell)} \quad \text{------ (8)}$$

where the coefficients c_i and b_ℓ are from Eq. (4), above. Here, α is the fine-structure constant, ω is the photon energy and the D's are the dipole matrix elements given by

$D_{nj\to j'} = i^{l\text{-}l}e^{i\delta_k}\left\langle \kappa \left\| Q_1^{(1)} \right\| \kappa_b \right\rangle$ **[explained in Ref. 12]** for the various possible $j \to j'$ transitions allowed by dipole selection rules. The angular distribution asymmetry parameter is given, for the i^{th} (or ℓ^{th}) configuration, by [12]:

$$\beta_{n\kappa}^{(i,\ell)}(\omega) = \frac{\left[\begin{array}{l} \frac{(2j\text{-}3)}{2(2j)}\left|D_{j\to j\text{-}1}\right|^2 - \frac{(2j\text{-}1)(2j+3)}{(2j)(2j+2)}\left|D_{j\to j}\right|^2 + \frac{(2j+5)}{2(2j+2)}\left|D_{j\to j+1}\right|^2 \\ -\frac{3}{2j}\left(\frac{(2j-1)}{2(2j+2)}\right)^{\frac{1}{2}}\left(D_{j\to j-1}D_{j\to j}^{*} + c.c\right) - \frac{3}{2}\left(\frac{(2j-1)(2j+3)}{(2j)(2j+2)}\right)^{\frac{1}{2}}\left(D_{j\to j-1}D_{j\to j+1}^{*} + c.c\right) \\ +\frac{3}{(2j+2)}\left(\frac{(2j+3)}{2(2j)}\right)^{\frac{1}{2}}\left(D_{j\to j}D_{j\to j+1}^{*} + c.c\right) \end{array}\right]}{\left|D_{j\to j-1}\right|^2 + \left|D_{j\to j}\right|^2 + \left|D_{j\to j+1}\right|^2} \quad \text{------ (9)}$$

with the net $\beta_{n\kappa}(\omega)$ for each subshell being given by $\beta_{n\kappa}(\omega) = \dfrac{\sum_{i=1}^{n_c} c_i^{\,2}\sigma_{n\kappa}^{(i)}\beta_{n\kappa}^{(i)} + \sum_{j=1}^{n_b} b_j^{\,2}\sigma_{n\kappa}^{(j)}\beta_{n\kappa}^{(j)}}{\sum_{i=1}^{n_c} c_i^{\,2}\sigma_{n\kappa}^{(i)} + \sum_{j=1}^{n_b} b_j^{\,2}\sigma_{n\kappa}^{(j)}}$.

III. Results and Discussion

The RRPA and RRPA-R calculations reported earlier [2] were repeated and reproduced first as a check, with a small difference in that we included additional channels from the 4s and 4p subshells, in addition to those from the 4d, 5s, 5p and 6s subshells employed earlier [2]. The addition of the 4s+4p channels does not, however, have any significant impact on the photoionization parameters of 4d subshell. The RRPA and the RRPA-R results presented in this work are the new results which include all relativistic dipole channels from 4s, 4p, 4d, 5s, 5p and 6s subshells. The photoionization cross sections and the photoelectron angular distributions presented in the figures below are from set 'b' calculation of RMCTD method as mentioned in section II. In this work, we report photoionization cross sections of the 4d subshell and also of the 6s, 5p and 5s subshells of atomic barium in the energy region in the neighborhood of the 4d ionization threshold. In addition, we present photoelectron angular distributions of the 4d and 5p photoelectrons.

A. 4d Subshell

The enhancement in the photoionization cross section due to the giant (shape) resonance [38] in the 4d subshell strongly influences the matrix elements for photoionization of other subshells in the energy region near the 4d delayed maximum *via* interchannel coupling. Kelly *et al.,* [4] have calculated the photoionization cross section of barium 4d subshell at the HF level, both with and without the inclusion of relaxation effects and found that the presence of relaxation effects broadened the peak in the 4d cross section (Fig 1); the RPAE photoionization cross section [1] in the near threshold region for 4d subshell overestimates the experimental cross section [5-7, 39] by about 60 Mb; RRPA brings the peak cross section down, (relative to RPAE), but nevertheless 25 Mb higher than the experimental data. Including relaxation effects, in addition to the relativistic effects (RRPA-R), the cross section is reduced further, getting close to the experimental value [2]; the remaining difference from experiment is probably due to the omission of double electron excitations in the calculation.

The 4d photoionization cross section for barium is considerably more sensitive to the inclusion of relativistic, relaxation and interchannel coupling effects compared to that for xenon, which is different from barium only in the absence of the 6s electrons [2]. This has been explained [2] in

terms of the extraordinary sensitivity of the double-well effective potential for an f-electron excited from the 4d subshell in Ba compared to Xe. In the case of atomic barium, the f-electron is on the verge of being able to bind an electron the inner well as in the lanthanides. This, of course, makes the 4d→f shape resonance in Ba very sensitive, since small changes in the potential alter the presence of f-electrons in one or the other potential well and, in turn, strongly affects the energy dependence of the photoionization cross section. The results of the various calculations for the Ba 4d photoionization cross section are shown in Fig. 1 where it is seen that the RMCTD (geometric mean of length and velocity) results are seen to be in reasonable agreement with experiment. It is clear that mixing the $6s^2$ outer shell configuration with $5d^2$ and $6p^2$ excited state diminishes the value of the 4d cross section to a considerable amount, compared to RPAE, RRPA and the RRPA-R, and brings the result into much better agreement with experiment. Results are presented on the photoelectron energy scale since the ionization thresholds obtained from the DHF, ΔE_{SCF} and GRASP-92 methods are different. The *total* 4d cross section presented is the sum of the $4d_{3/2}$ and $4d_{5/2}$ cross sections.

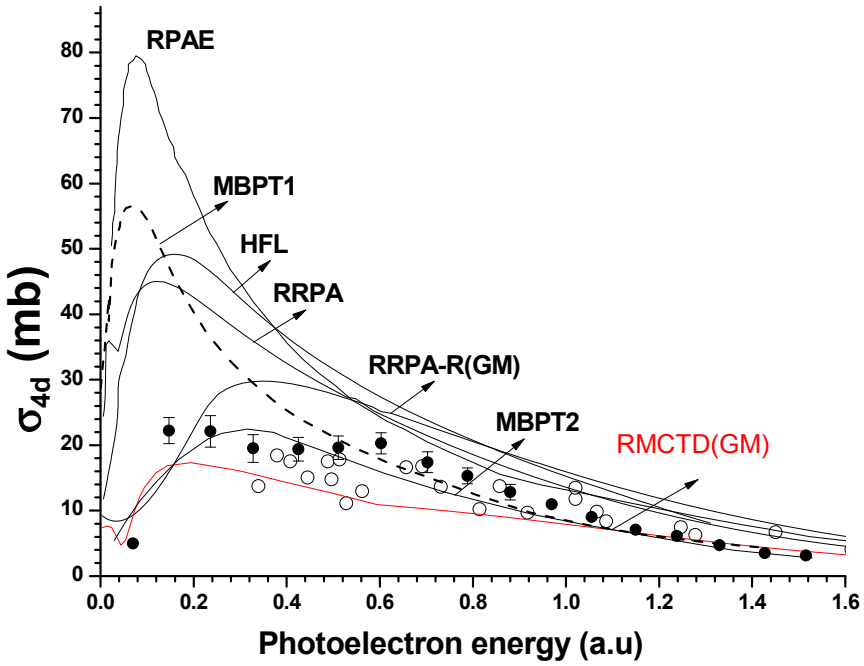

Fig 1: Ba 4d photoionization cross section *vs*. photoelectron energy. Theoretical results shown are the geometric mean of the present RMCTD results, labelled RMCTD (GM), along with RPAE [1], HF-Length (HFL) [4], RRPA [2], the geometric mean of RRPA with relaxation, RRPA-R (GM) [2], and the length forms of MBPT [3] without relaxation (MBPT1) and with relaxation and polarization (MBPT2). The solid circles are the

experimental results of Ref. [5] and open circles are from Ref. [6].

From the comparison it is clear that most of the methodologies predict a 4d cross section that is too large, sometimes grossly. E.g., the maximum in the RPAE cross section is a factor of four larger than experiment. The cross section is lowered by the introduction of relativistic effects; the RRPA result is half of the RPAE cross section. Relaxation, interchannel coupling and initial-state correlation all seem to be of some importance. It is of interest to note that the MBPT2 calculation [3] also gives reasonably good agreement with experiment, despite being entirely nonrelativistic. It is to be noted that and RPAE-based calculation that included core rearrangement and relaxation [1] (not shown) also gave reasonable agreement with experiment even though it too was nonrelativistic. In any case, however, the RMCTD (GM) methodology apparently contains all of the important physics to reproduce the experimental cross section in a satisfactory manner.

The angular distribution asymmetry parameter, β_{4d}, is presented in Fig. 2 for RRPA, the RRPA-R and the RMCTD methods.. For a spin-orbit-split nl shell, β_{nl} is the weighted average [12] $\beta_{nl} = \frac{\sum_\kappa \sigma_{n\kappa}\beta_{n\kappa}}{\sum_\kappa \sigma_{n\kappa}}$; for the 4d subshell, we have $\beta_{4d} = \frac{\sigma_{4d_{3/2}}\beta_{4d_{3/2}} + \sigma_{4d_{5/2}}\beta_{4d_{5/2}}}{\sigma_{4d_{3/2}} + \sigma_{4d_{5/2}}}$. Above the threshold region, all the theories are in reasonably good agreement with the experimental data. The length and velocity form (not shown individually) are fairly close to each other in RMCTD method.

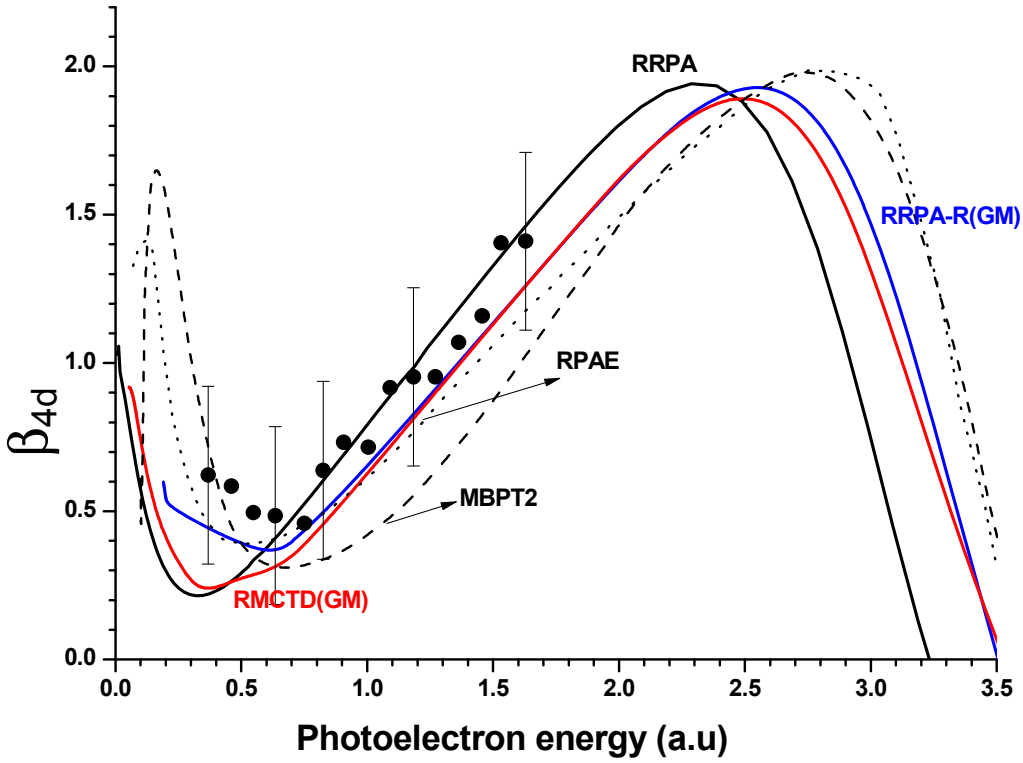

Fig 2: Ba 4d photoelectron angular distribution β parameter shown along with various theoretical results. Shown are the present RMCTD, which is the geometric mean of length and velocity forms, denoted as RMCTD (GM), RPAE [1], MBPT2, which includes relaxation and polarization effects [3], RRPA and RRPA-R (GM), which are the results of the present work, as described in the text.

Unlike the case of the cross sections, all of the theoretical results for β are in rather good agreement with each other, and also with experiment, except for some differences near the threshold. β is determined by the ratio of the magnitudes of the 4d→f and 4p→d matrix elements, along with the phase difference of the matrix elements [43]. The RPAE and the present RMCTD (GM) results for the photoelectron angular distribution parameter are in relatively good agreement compared to the comparison of the corresponding cross sections. This is presumably because of the fact that the photoelectron angular distribution asymmetry parameter is given by a ratio in which the differences in the cross section get cancelled out.

B. 5s, 5p and 6s Subshells

The Ba 5s photoionization cross section, shown in Fig. 3, is very strongly affected by correlation; specifically, correlation in form of interchannel coupling [40, 41] with the 4d photoionization channels. To fully appreciate the dramatic effect of the correlation, the RMCTD length and velocity cross sections were also determined *without* coupling the 4d photoionization channels. The results, without the 4d-channels coupled are labelled in Fig. 3 as RMCTD0, and are found to be very tiny over the entire range of energies, no more than a few hundredths of a Mb; with the coupling, however, the RMCTD result is seen to be almost two orders of magnitude larger. In other words, the single-particle cross section is essentially irrelevant, in this case, and the Ba 5s cross section is completely dominated by interchannel coupling with the 4d channels. And it is also clear from Fig. 3 that the RMCTD (GM) cross section is in reasonable quantitative agreement with experiment, which the RRPA, MBPT and RRPA-R are not. Note that in Fig. 3, for purposes of comparison, the various theoretical curves have been shifted horizontally to match their $4d_{3/2}$ threshold (or 4d for nonrelativistic calculations) with the experimental $4d_{3/2}$ threshold. The discontinuities in the theoretical curves are the autoionization regions which are omitted in the plot to simplify comparison. Note further that the RPAE-R result, which is RPAE plus rearrangement and relaxation taken into account exhibits quite good agreement with experiment even though it is nonrelativistic.

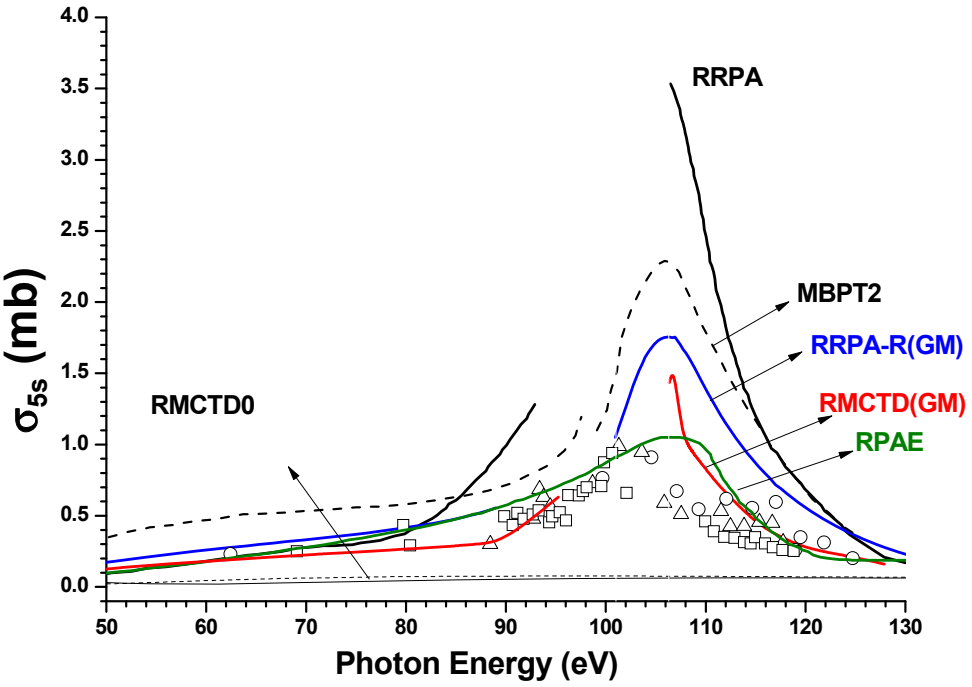

Fig 3: Ba 5s photoionization cross section in the region of the 4d thresholds. The theoretical curves are labelled as in Fig. 1 with the addition of the RMCDT0 results in which the coupling with the 4d photoionization channels is omitted in length (solid line) and velocity (dashed line) formulations, and RPAE-R, which is RPAE with the addition of rearrangement and relaxation [45]. The discontinuities in the theoretical curves are owing to the omission of the regions of autoionizing resonances below the 4d thresholds which have been left out to simplify the comparisons. The theoretical curves are shifted by the difference between the theoretical and experimental $4d_{3/2}$ thresholds. The experimental results shown are open circles [5], open triangles [6] and open squares [44].

The calculated RMCTD 5p photoionization cross section, the sum of the $5p_{1/2}$ and $5p_{3/2}$ cross sections, is shown in Fig. 4 along with the results of several other calculations and experiment. As with the 5s, the 5p cross section is dominated by the interchannel coupling with 4d photoionization channels. The experimental data is seen to be a bit scattered, e.g., at around 95 eV the highest experimental point is a factor of three larger than the smallest, well outside the stated error bars. Owing to this experimental scatter, it is difficult to assess the RMCTD results fully, but they are seen to be in the right ballpark. Better experimental data here would be most useful. In any case, the RRPA-R (GM) seems to give the best agreement

with experiment, slightly better than RMCTD (GM) which seems to indicate that not all important initial state correlations have been taken into account in RMCTD.

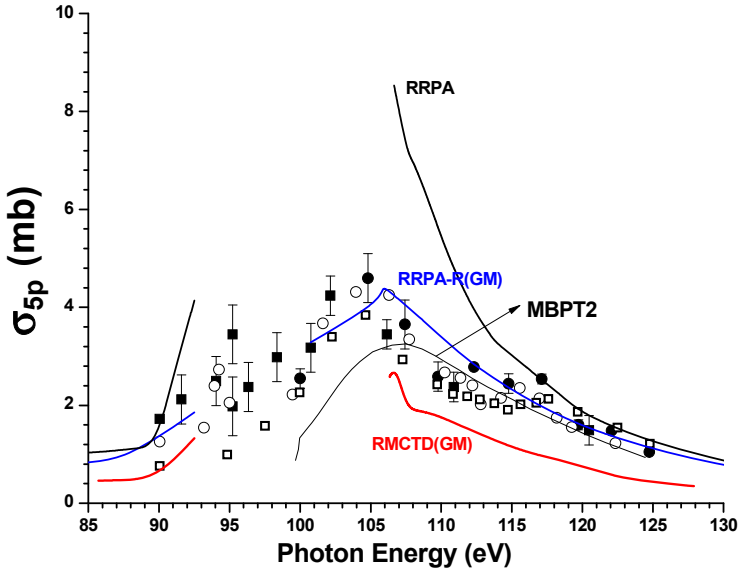

Fig 4: Ba 5p photoionization cross section. The theoretical curves are labelled as in Fig. 1 with the discontinuities leaving out the autoionization resonances. Experiment is given by closed squares [6], closed circles [5] and open circles [44]. The theoretical curves are shifted by the difference between the theoretical and experimental $4d_{3/2}$ thresholds.

The angular distribution asymmetry parameter, β, for the 5p subshell obtained from the RRPA, RRPA-R and the RMCTD methods are shown in Fig. 5. The β for the spin-orbit split np subshell is calculated exactly as described for the 4d β case, i.e. by taking a weighted average of the asymmetry parameters of $p_{1/2}$ and $p_{3/2}$ subshells. The RRPA and RRPA-R calculations are done by including all dipole channels from the 4s+4p+4d+5s+5p+6s subshells. Results are presented at different levels of truncation of RMCTD method. In all the theories, we note that interchannel coupling with channels from the 4d subshell is necessary to get agreement with the experiment; results which omit that coupling disagree with experiment strongly. Thus the RMCTD results in which coupling with 4d channels is omitted is not in good agreement with experiment, whereas the RMCTD calculation inclusive of 4d coupling is in good agreement. We observe that the agreement between theory and experiment for the angular distribution asymmetry parameter is somewhat better in the case of 4d photoionization compared to that of 5p. The 4d β is determined by the interference between $d \rightarrow f$ and $d \rightarrow p$ channels and the relative strength is strongly in favor of the $d \rightarrow f$ channels. In the case of the 5p β which is

determined by the interference between $p \rightarrow d$ and $p \rightarrow s$ the relative strength of the $p \rightarrow d$ channels is comparably not that much stronger than $p \rightarrow s$ channel as is the case with 4d β. So therefore any neglect of detail correlation is of less importance in the case of 4d β compared to 5p β.

The length and velocity forms of the RMCTD method are fairly close to each other. The geometric mean of the two forms is given for RRPA-R and RMCTD methods in Fig. 5. The RMCTD calculation of β is in very good agreement with the experiment, which means that the relative phases of the various partial waves are accurate, and that the Cooper minimum is at the correct location. Again, it would good to have experiment over a broader range of energies for a more extensive comparison to test theory.

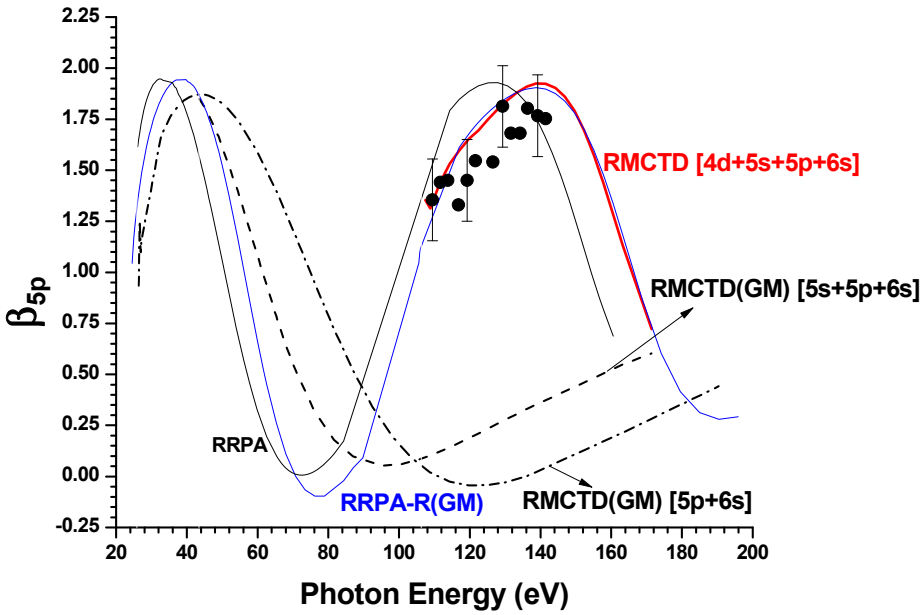

Fig 5: Ba 5p photoelectron angular distribution parameter β with the theoretical curves labelled as Fig. 1, except that the RMCTD (GM) results are shown for several different levels on truncation, as indicated. The experimental values are from Ref. [5].

The RMCTD Ba 6s photoionization cross section is shown in Fig. 6 along with several other theoretical results and experiment. The cross section is quite small, maximizing at less than 0.2 Mb in this energy region; however, it is much larger than the cross section calculated without coupling with the 4d photoionization channels. Thus, as in the cases of 5s and 5p, the maximum in the cross section in the 100 eV region is entirely due to interchannel coupling with the 4d

channels. Also, as in the previous cases, the calculations are entirely *ab initio* except for a shift in energy so that the calculated $4d_{3/2}$ threshold aligns with the experimental. The RMCTD (GM) cross section is in rather good agreement with experiment, especially in the higher-energy region, and the overall agreement with experiment is better than the RRPA, RRPA-R or MBPT results as seen in Fig. 6. It must be pointed out, however, that the experimental results exhibit significant scatter and large error bars; more accurate experimental data would be most helpful in assessing theory.

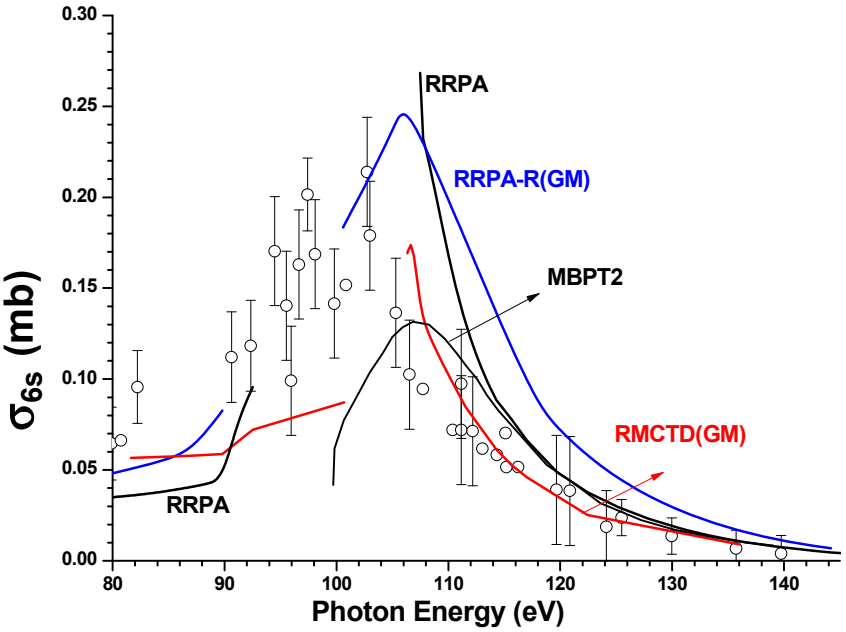

Fig 6: Ba 6s photoionization cross section. Theoretical curves as Fig. 1, experiment, Ref. [6]. The theoretical curves are shifted by the difference between the theoretical and experimental $4d_{3/2}$ thresholds.

IV. Conclusions

Analysis of the photoionization of atomic Ba is a challenging problem on account of the many-electron correlations which contribute to the details of its experimental features. Unlike the Xe atom [14] for which the RRPA results are in quite good agreement with experiment for 4d photoionization, the RRPA results for Ba overestimated the experimental cross sections [2]. The present RMCTD results, which include non-RPA correlations from the use of a MCDHF initial state wave function and various dipole ionization and excitation channels originating from the multiconfigurational initial state,

provides the best agreement with the available experimental data in the following cases: (a) the 4d cross section (with respect to the experimental results of Bizau *et al.* [6], although the MBPT results agree better with the experimental results of Becker *et al.,*[5]); even as both RMCTD and the MBPT results give good agreement at higher energies with both sets of experimental data; (b) the 5s cross section in the energy region below the 4d threshold, as well as in the energy region well above the 4d threshold; (c) the 6s cross section above the 4d threshold. The RMCTD results for the photoelectron angular distribution asymmetry parameters β are also in best agreement with experimental data compared to other theoretical models in the following cases: (a) the 4d β, although RRPA-R gives equally good agreement; (b) the 5p β above the 4d threshold. In the case of some other features of the spectra, some of the other theoretical models give somewhat better agreement with the experiment. For example, the RPAE-R gives the best agreement with regard to the 4d cross section at its threshold. Overall, however, RMCTD results are in best agreement with the data in the largest number of cases.

The present work demonstrates the utility of the RMCTD method in hitherto untested applications and projects it as a competitive relativistic many-body methodology for the analysis of atomic photoionization processes. An added advantage which the RMCTD method has above the RPA/RRPA methods is the fact that it can also be used to study open-shell atoms and ions since both the multi-configuration expansion of the initial state wave functions and the Tamm-Dancoff multichannel final state wave functions are admissible in the RMCTD method.

Acknowledgments

The work of STM was supported in part by the US Department of Energy, Basic Energy Sciences, Division of Chemical Sciences. The travel of PCD to Georgia State University was supported by NSF. AG's work was supported by the Department of Science and Technology, Government of India. The referee's critical comments have helped us significantly improve the manuscript.

References

[1] M. Ya. Amusia, V. K. Ivanov and L.V. Chernysheva, Phys. Lett. **59A,** 191 (1976).
[2] V. Radojević, M. Kutzner and H. P. Kelly, Phys. Rev. A **40,** 727 (1989).
[3] M. Kutzner, Z. Altun and H. P. Kelly, Phys. Rev. A **41**, 3612 (1990).
[4] H. P. Kelly, S. L. Carter, and B. E. Norum, Phys. Rev. A **25**, 2052 (1982).
[5] U. Becker, D. Szostak, H.G. Kerkhoff, M. Kupsch, B. Langer, R. Wehlitz, A. Yagishita, and T. Hayaishi, Phys. Rev. A **39**, 3902 (1989).
[6] J. M. Bizau, D. Cubaynes, P. Gerard, and F. J. Wuilleurnier Phys. Rev. A **40**, 3002 (1989).
[7] J. M. Bizau, D. Cubaynes, J.-M. Esteva, F. J. Wuilleumier, C. Blancard, J. Bruneau, J.-P. Champeaux, A. Compant La Fontaine, C. Couillaud, R. Marmoret, C. Rémond, D. Hitz, M. Delaunay, N. Haque, P. C. Deshmukh, H. L. Zhou, and S. T. Manson, Phys. Rev. Lett. **87**, 273002 (2001).
[8] S. B. Whitfield, R. Wehlitz and V. K. Dolmatov, J. Phys. B **44,** 165002 (2011).
[9] A. Zangwill and P. Soven, *Phys. Rev. Lett*. **45**, 204 (1980).
[10] U. Fano and J. W. Cooper*,* Rev. Mod. Phys. **40**, 441 (1969).
[11] A. F. Starace, in Handbuch der Physik, ed. by. W. Mehlhorn (Springer, Berlin, 1982), **31**, pp. 1-121.
[12] W. R. Johnson and C. D. Lin, Phys. Rev. A **20**, 964 (1979).
[13] V. Radojević and W. R. Johnson, Phys. Rev. A **31,** 2991 (1985).
[14] W. R Johnson and K. T. Cheng, Phys. Rev. A **20**, 978 (1979).
[15] N. Shanthi, P. C. Deshmukh, and S. T. Manson, Phys. Rev. A **37**, 4720 (1988).
[16] G. B. Pradhan J. Jose, P. C. Deshmukh, V. Radojević, and S. T. Manson, Phys. Rev. A **81**, 063401 (2010).
[17] P. C. Deshmukh and W. R. Johnson, Phys. Rev. A **27**, 326 (1983).
[18] P. C. Deshmukh and W. R. Johnson, Phys. Rev. A **28**, 209 (1983).
[19] P. C. Deshmukh, V. Radojević and S. T. Manson, Phys. Rev. A **45**, 6339 (1992).
[20] H. R. Varma, T. Banerjee, S. Sunil Kumar, P. C. Deshmukh, V. K. Dolmatov and S. T. Manson*,* J Phys. Conf. Ser. **80**, 012025 (2007).
[21] N. Shanthi, J. Phys. B **21,** L427 (1988).
[22] P. Shorer and A. Dalgarno, Phys. Rev. A **16**, 1502 (1977).
[23] V. Radojević and W. R. Johnson, J. Phys. B **16**, 177 (1983).
[24] M. Kutzner and V. Radojević, Phys. Rev. A **49**, 2574 (1994)
[25] P. C. Deshmukh, V. Radojević, and S. T. Manson*,* Phys. Lett. A **117**, 293 (1986).
[26] C. M. Lee and W. R. Johnson, Phys. Rev. A **22**, 979 (1980).
[27] H. Beutler, Z. Phys. **93**, 177 (1935); U. Fano, Nuovo Cimento **12**, 154 (1935).
[28] M. Nrisimhamurty G. Aravind, P. C. Deshmukh and S. T. Manson*,* Phys. Rev. A **91**, 013404 (2015).
[29] F. A. Parpia, C. Froese Fischer and I. P. Grant, Comput. Phys. Commun. **94**, 249 (1996).
[30] G. B. Pradhan, J. Jose, V. Radojević, S. T. Manson and P. C. Deshmukh*,* J Phys. Conf. Ser. **194**, 022042 (2009).
[31] G. Aarthi, J. Jose, S. Deshmukh, V. Radojević, P. C. Deshmukh and S. T. Manson, J. Phys. B **47,** 025004 (2014).
[32] V. Radojević, J. Jose, G. B. Pradhan, P. C. Deshmukh and S. T. Manson*,* Publ. Astron. Obs. Belgrade **89**, 29 (2010).
[33] J. Jose, G. B. Pradhan, V. Radojević, S. T. Manson, and P.C. Deshmukh*,* Phys. Rev. A **85**, 053419 (2011).
[34] G. Snell, M. Martins, E. Kukk, W. T. Cheng, and N. Berrah*,* Phys. Rev A **63**, 062715 (2001).

[35] I. P. Grant, J Phys. B **43**, 074033 (2010).
[36] http://www.nist.gov/pml/data/asd.cfm
[37] A. Derevianko, W. R. Johnson and K. T. Cheng, At. Data Nuc. Data Tables **73**, 153 (1999).
[38] J. P. Connerade, J. M. Esteva and R. C. Karnatak (eds.), Giant Resonances in Atoms, Molecules and Solids, Vol 151 of NATO Advanced Study Institute, Series B: Physics (Plenum, New York, 1987).
[39] M. H. Hecht and I. Lindau, Phys. Rev. Lett. **47**, 821 (1981).
[40] E. W. B. Dias, H. S. Chakraborty, P. C. Deshmukh, S. T. Manson, O. Hemmers, P. Glans, D. L. Hansen, H. Wang, S. B. Whitfield, D. W. Lindle, R. Wehlitz, J. C. Levin, I. A. Sellin and R. C. C. Perera, Phys. Rev. Lett. **78**, 4553 (1997).
[41] D. L. Hansen, O. Hemmers, H. Wang, D. W. Lindle, I. A. Sellin, H. S. Chakraborty, P. C. Deshmukh and S. T. Manson, Phys. Rev. A **60**, R2641 (1999).
[42] J. Jose, G. B. Pradhan, V. Radojevic, S. T. Manson and P. C. Deshmukh, Phys. Rev. A **83**, 053419 (2011).
[43] S. T. Manson and A. F. Starace, Rev. Mod. Phys. **54**, 389 (1982).
[44] M. Richter, M. Meyer, M. Pahler, T. Prescher, E. V. Raven, B. Sonntag, and H. E. Wetzel, Phys. Rev A, **39**, 5666 (1989).
[45] M. Ya. Amusia, Adv. At. Molec. Phys. **17**, 1 (1981) and references therein.